

# Kinetic and thermodynamic sorption studies of Fe(III) and Zr(IV) by DFO@Purolite, a desferrioxamine B based chelating resin

Giancarla Alberti,\*<sup>a</sup> Camilla Zanoni,<sup>a</sup> Vittorio Losi,<sup>a</sup> Sara Rovertoni,<sup>a</sup> Lisa Rita Magnaghi,<sup>a</sup> Osian Fonquerne,<sup>b</sup> Stéphane Brandès,<sup>b</sup> Agnese Amati,<sup>c</sup> Jean-Claude Chambron,<sup>c</sup> Nicolas Maudoux,<sup>d</sup> Raffaela Biesuz,<sup>a</sup> and Michel Meyer\*<sup>b</sup>

<sup>a</sup> Dipartimento di Chimica - Università degli Studi di Pavia, via Taramelli 12, 27100 Pavia, Italy

<sup>b</sup> Institut de Chimie Moléculaire de l'Université de Bourgogne (ICMUB), UMR 6302, CNRS, Université de Bourgogne, 9 avenue Alain Savary, BP 47870, 21078 Dijon Cedex, France

<sup>c</sup> Institut de Chimie de Strasbourg, UMR 7177, CNRS, Université de Strasbourg, 1 rue Blaise Pascal, BP 296 R 8, 67008 Strasbourg Cedex, France

<sup>d</sup> TrisKem International, 3 rue des Champs Géons, ZAC de l'Éperon, 35170 Bruz, France

## Supplementary Information

## **Contents**

I.	Infrared spectroscopy	3
II.	Thermogravimetric analyses (TGA)	4
III.	Scanning electron microscopy (SEM)	5
IV.	Luminescence emission spectroscopy	6
V.	Two-photon microscopy	7
VI.	Auxiliary equilibrium constants	8

## I. Infrared spectroscopy

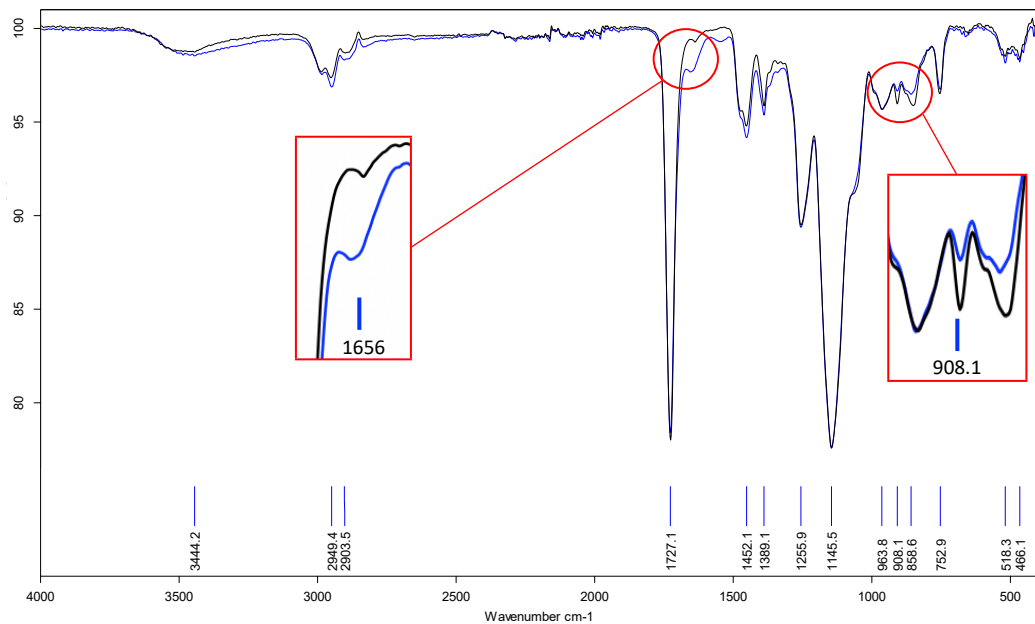


**Figure S1.** ATR FT-MIR spectra of pristine Purolite® ECR8209 (black line) and DFO@Purolite (red line) recorded at a resolution of 4 cm<sup>-1</sup>.

## II. Thermogravimetric analyses (TGA)

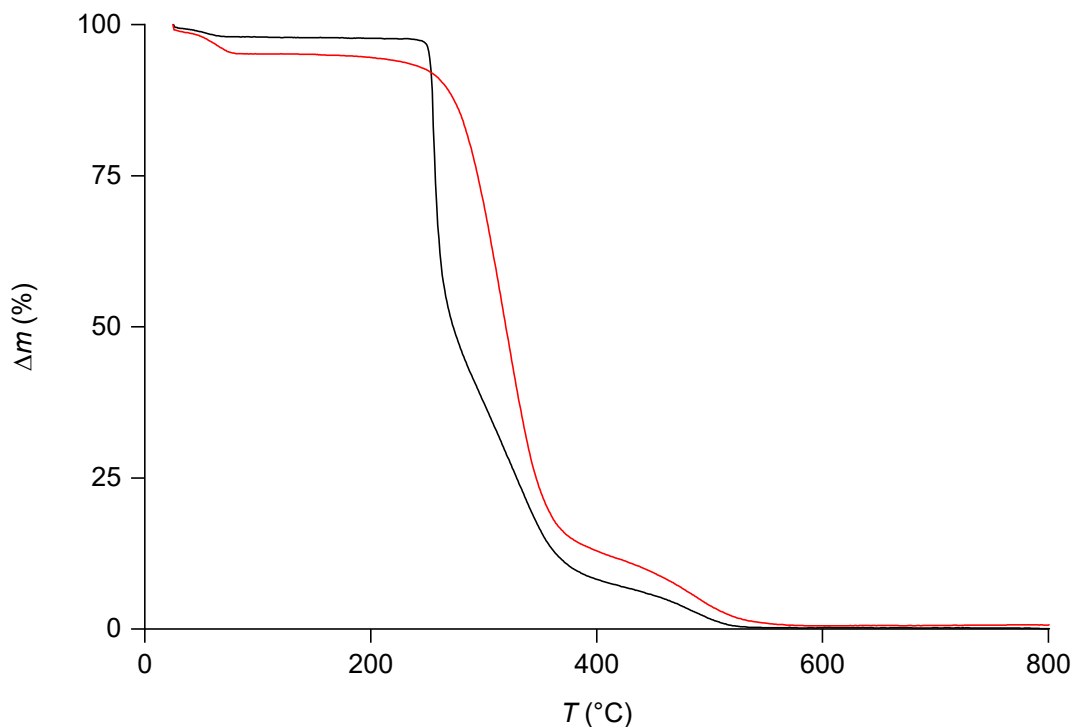


**Figure S2.** Thermograms of pristine Purolite<sup>®</sup> ECR8209 (black line) and DFO@Purolite (red line) recorded under a N<sub>2</sub> (30 mL min<sup>-1</sup>)/O<sub>2</sub> (10 mL min<sup>-1</sup>) gas stream at a heating rate of 10 °C min<sup>-1</sup>.

### III. Scanning electron microscopy (SEM)

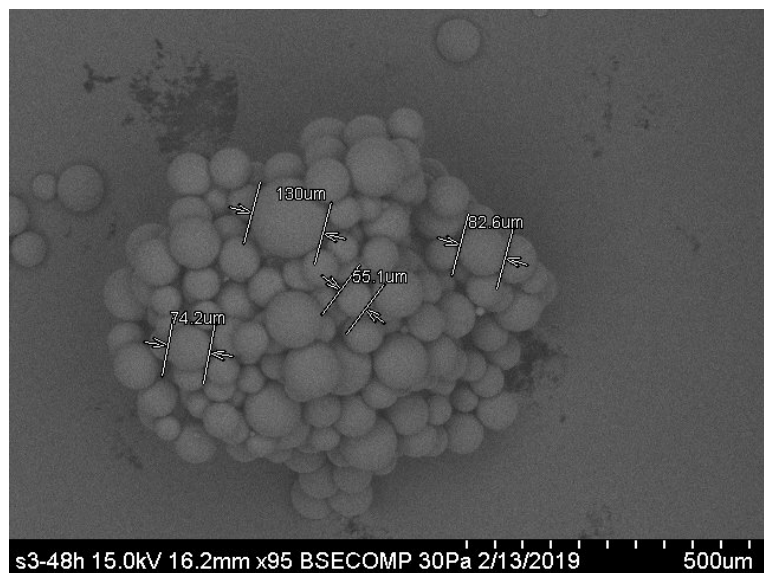


**Figure S3.** SEM image of gold-sputtered Purolite® ECR8209 resin. Magnification: ×95, working distance: 16.2 mm, acceleration voltage: 15.0 kV, vacuum: 30 Pa.

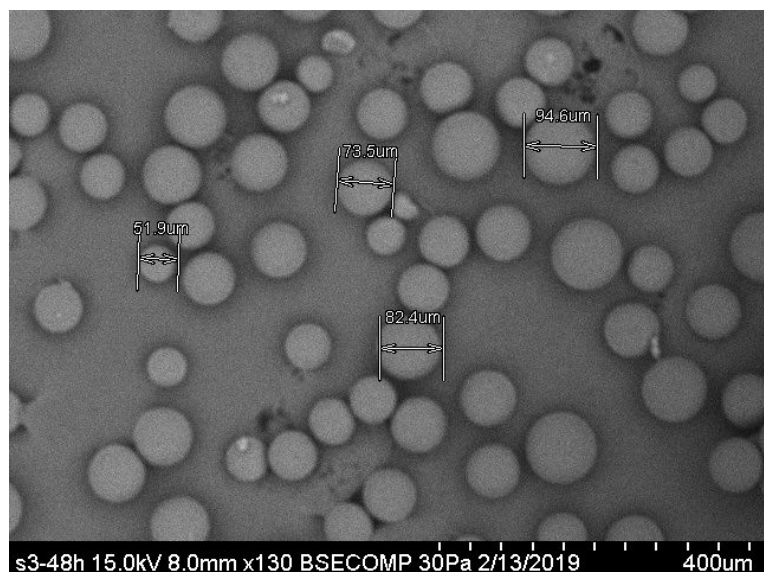


**Figure S4.** SEM image of gold-sputtered DFO@Purolite resin. Magnification: ×130, working distance: 8.0 mm, acceleration voltage: 15.0 kV, vacuum: 30 Pa.

#### IV. Luminescence emission spectroscopy

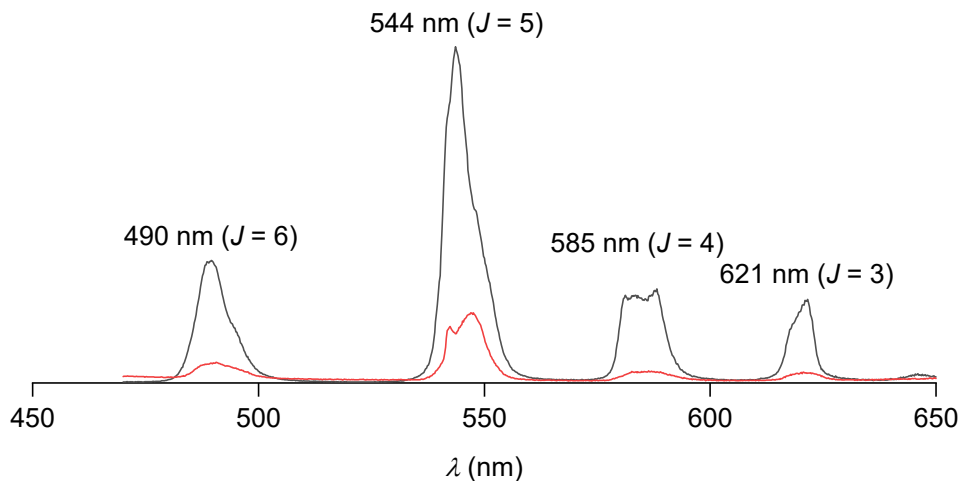


**Figure S5.** Emission spectra of a 0.015 M  $\text{Tb}(\text{NO}_3)_3$  solution in 0.01 M  $\text{HNO}_3$  showing the  ${}^5\text{D}_4 \rightarrow {}^7\text{F}_J$  transitions (black line) and of  $[\text{Tb}(\text{DFO})\text{H}]^+$  at pH 9.6 (red line).  $\lambda_{\text{ex}} = 355$  nm.

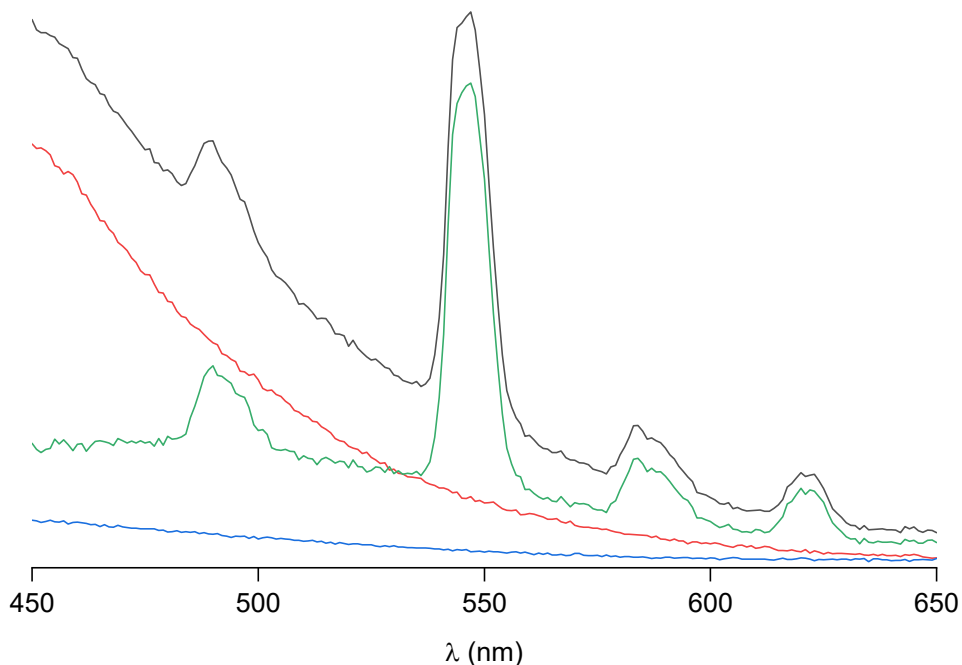


**Figure S6.** Emission spectra of pristine Purolite® ECR8209 (blue line), DFO@Purolite (red line), and  $\text{Tb}(\text{DFO})@\text{Purolite}$  (black line) resins. The green line corresponds to the  $\text{Tb}(\text{DFO})@\text{Purolite}$  spectrum after subtraction of the DFO@Purolite contribution.  $\lambda_{\text{ex}} = 355$  nm, entrance and exit slit bandpass: 2 nm.

## V. Two-photon microscopy

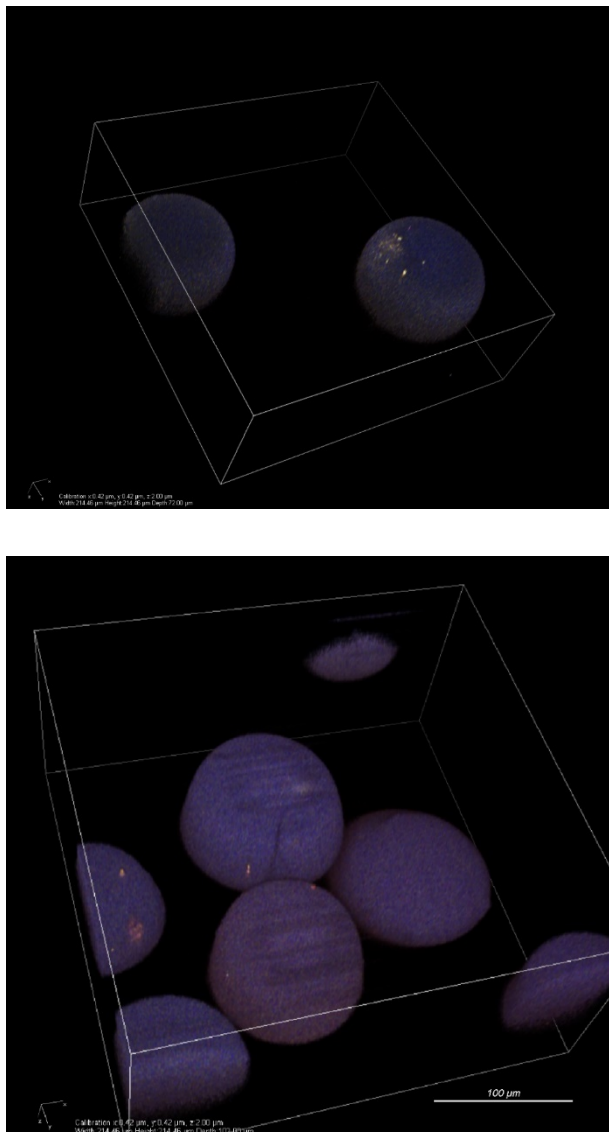


**Figure S7.** Two-photon microscopy images of DFO@Purolite (top) and Tb(DFO)@Purolite (bottom) beads showing the autofluorescence of DFO and luminescence of Tb(III), respectively, upon excitation at 750 nm by a NIR laser. Pictures collected on each of the four detection channels (400–492, 500–550, 563–588, 601–657 nm) were merged without any other spectral selection. The 3D z-stack views were constructed by superimposing the resulting images scanned along the depth (100  $\mu\text{m}$ ) of the samples.

## VI. Auxiliary equilibrium constants

**Table S1.** Values of the global protonation constants ( $\beta^{\circ}_{01z}$ ) of  $\text{EDTA}^{4-}$ , of the hydrolysis ( $\beta^{\circ}_{x0z}$ ) and complex formation constants ( $\beta^{\circ}_{xyz}$ ) with  $\text{EDTA}^{4-}$  of  $\text{Fe}^{3+}$  and  $\text{Zr}^{4+}$  at infinite dilution retrieved from the database implemented in the MEDUSA software.<sup>a</sup>

	$x$	$y$	$z$	$\log \beta_{mlh}$
$\text{HEDTA}^{3-}$	0	1	1	11.24
$\text{H}_2\text{EDTA}^{2-}$	0	1	2	18.04
$\text{H}_3\text{EDTA}^{-}$	0	1	3	21.19
$\text{H}_4\text{EDTA}$	0	1	4	23.42
$\text{H}_5\text{EDTA}^{+}$	0	1	5	22.12
$\text{H}_6\text{EDTA}^{2+}$	0	1	6	21.62
$\text{H}_4\text{EDTA}_{(s)}$	0	1	4	27.22
$\text{Fe}(\text{EDTA})^{-}$	1	1	0	27.8
$\text{Fe}(\text{HEDTA})$	1	1	1	29.3
$\text{Fe}(\text{EDTA})(\text{OH})^{2-}$	1	1	-1	19.97
$\text{Fe}_2(\text{EDTA})_2(\text{OH})_2^{4-}$	2	2	-2	41.8
$\text{Fe}(\text{OH})^{2+}$	1	0	-1	-2.19
$\text{Fe}(\text{OH})_2^{+}$	1	0	-2	-5.67
$\text{Fe}(\text{OH})_3$	1	0	-3	-12.56
$\text{Fe}(\text{OH})_4^{-}$	1	0	-4	-21.6
$\text{Fe}_2(\text{OH})_2^{4+}$	2	0	-2	-2.95
$\text{Fe}_3(\text{OH})_4^{5+}$	3	0	-4	-6.3
$\text{Fe}(\text{OH})_{3(\text{am})}$	1	0	-3	-4.891
$\text{Fe}_2\text{O}_3(\text{cr})$	2	0	-6	-0.408
$\text{FeOOH}_{(s)}$	1	0	-3	-1
$\text{Zr}(\text{EDTA})$	1	1	0	31.1
$\text{Zr}(\text{OH})^{3+}$	1	0	-1	0.3
$\text{Zr}(\text{OH})_2^{2+}$	1	0	-2	-1.7
$\text{Zr}(\text{OH})_3^{+}$	1	0	-3	-5.1
$\text{Zr}(\text{OH})_4$	1	0	-4	-9.7
$\text{Zr}_3(\text{OH})_4^{8+}$	3	0	-4	-0.6
$\text{Zr}_4(\text{OH})_8^{8+}$	4	0	-8	6
$\text{ZrO}_{2(s)}$	1	0	-4	-1.9

<sup>a</sup> I. Puigdomenech, MEDUSA – Chemical Equilibrium Diagrams Program, (2010), Royal Institute of Technology: Stockholm, Sweden (<https://www.kth.se/che/medusa/>).